Fabrication and Characterization of UN-USi$_x$ Nuclear Fuel

Alicia Marie Raftery

Supervisor:

Dr. Mikael Jolkkonen

Examiner:

Dr. Janne Wallenius

Spring 2015

"What I cannot create, I do not understand."

Richard P. Feynman

Abstract

In this thesis, UN-U_3Si_2 nuclear fuel was fabricated using spark plasma sintering and characterized to analyze the microstructure and crystal structure of the resulting pellets. This work was done in collaboration with accident tolerant fuel research, an effort which aims at developing nuclear fuel with superior safety and performance compared to currently used oxide fuels.

Uranium silicide was manufactured by arc melting to produce U_3Si_2 and uranium mononitride was synthesized by using the hydriding-nitriding method. They were mixed in varying compositions (5 wt%, 10 wt%, 20 wt%, and 25 wt% U_3Si_2) in order to create composite fuel pellets. Characterization of the resulting pellets showed an apparent ternary phase of U-N-Si, prompting fabrication of four more pellets at varying temperatures ($1200\,°C$, $1300\,°C$, $1400\,°C$, and $1500\,°C$) to try and identify the temperature of phase formation.

The presence of a probable ternary U-N-Si phase was confirmed to be present in all fuel pellets. Therefore, further investigation into the thermodynamic behavior of the ternary U-N-Si system is suggested before this fuel can be recommended for use in a reactor.

Acknowledgments

There are many people who have helped me, both directly and indirectly, during the course of this project; the following few words are the least I can do to express my gratitude.

Thanks to Mikael Jolkkonen and Janne Wallenius, both of whom were there for guidance and important discussions during the development of this work.

Special thanks to Kyle Johnson - who went from my teacher to my lab partner to my friend. It is no exaggeration to say that nothing on the following pages would have been possible without him.

Thanks to my family and friends back in Texas who put up with my globetrotting ways, y'alls love and support mean everything to me.

And finally, to all of the KTH professors and staff who took time out of their day to pass on some knowledge to a curious student - Tack så mycket.

Contents

List of Figures

Chapter 1

Introduction

1.1 Accident Tolerant Fuel

Since the development of nuclear power in the 1950's, many different materials have been considered for use as nuclear fuel. The fuel element is essentially the core of a nuclear reactor, as it is responsible for producing the heat that is eventually converted into electricity. The success of nuclear power as a safe, economical, and reliable source of energy is therefore dependent upon the performance of the fuel. For this reason, many considerations go into the fuel design, including the behavior during normal reactor operation to behavior during potential accident conditions.

It is perhaps inherent to the field of engineering that vast improvements in design are made after the occurance of an accident. In the same way, the nuclear power industry is continuously enhancing the safety of nuclear power plants, taking accidents as an opportunity to identify and eliminate weaknesses in design. After the Fukushima Daiichi nuclear power plant suffered a severe accident in Japan in 2011, a high priority was placed on the pursuit of a light water reactor (LWR) fuel system that can withstand severe accident conditions. The hope is that significant improval in the fuel and cladding properties can delay the onset of detrimental reactions, and therefore increase the coping time to respond to an accident [1].

The key requirement for this so-called accident tolerant fuel (ATF) is the ability to handle a loss of active cooling in the core for a longer time period compared to the existing UO_2-zircaloy fuel system. At the same time, the fuel system must maintain or improve current fuel performance during normal operating conditions. Changes to both the fuel and cladding materials are being considered in order to meet this goal. The main foreseen fuel performance improvements are enhanced fission product retention at

high temperatures and improved thermal/mechanical physical properties. Several materials and designs with these superior properties are currently under investigation, including UN-USi composite fuel.

1.2 UN-USi$_x$ Composite Fuel

Uranium nitride and uranium silicide fuels have been studied for a number of years as two separate fuel concepts. The advantage of these fuels compared to uranium oxide fuel has been well established. However, the idea to create a composite fuel containing both uranium nitride and uranium silicide is relatively new.

Uranium nitride fuel refers to the use of uranium mononitride (UN) as a nuclear fuel, which exhibits a number of favorable properties compared to oxides. For instance, uranium nitride has a higher thermal conductivity, melting temperature, and fissile density [2]. The enhanced heat removal capabilities have made nitride fuel a promising potential fuel for future generation IV fast reactors. However, uranium nitride has a weakness when considered for use in light water reactors (LWRs); studies have shown that the corrosion rate of the fuel with steam may be unacceptable [3]. Oxidation resistance is desired because of the possibility that the fuel itself may be exposed to steam from the primary circuit during a severe accident scenario.

Research into uranium silicide fuels accelerated when the US Department of Energy began the Reduced Enrichment for Research and Test Reactors (RERTR) program in 1978, which aimed at converting the research reactors to using a lower enriched fuel for non-proliferation purposes. The goal of lower enrichment required the fuel to have a much higher fissile density, which sparked interest into the higher density uranium silicides [4]. Mixed results have been reported from the research into silicides, with swelling under irradiation identified as a possible problem, specifically for the high density U$_3$Si [5].

The purpose of creating a fuel with both uranium silicide and uranium nitride is the expectation that the composite could have more favorable properties. Most importantly, the silicide may provide oxidation tolerance through the formation of a protective layer of SiO$_2$ when exposed to air or steam [6]. For this to happen, the silicide phase should be essentially coating the surface of the nitride particles. Liquid phase sintering is a common method used to achieve this wetting effect, with recent research showing that spark plasma sintering allows even greater enhancement in particle rearrangement [7].

1.3   Spark Plasma Sintering

Spark plasma sintering (SPS) is a method used for powder consolidation through the means of applied pressure and electrical current. The advantages associated with SPS compared to other sintering methods include lower sintering temperatures, shorter holding times, and improved mechanical properties [9]. For this method of sintering, powders are loaded into a graphite die and heated by passing a DC electrical current through the die while simultaneously applying a uniaxial pressure. The schematic for the method is shown in Figure 1.1.
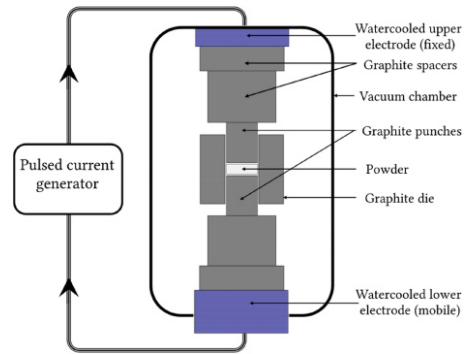
Figure 1.1: Schematic for spark plasma sintering method [10].

The discovery that sintering could be accomplished using an electrical current is documented in reports from as early as the 1930's [8]. However, research in this field has increased dramatically in the last 25 years due to increased availability of equipment. Based on numerous studies, it is clear that SPS delivers the ability to sinter in a matter of minutes and at temperatures $200 - 500\,^{\circ}$C lower than conventional methods of sintering [11]. Yet, currently there exists no clear explanation of the specific mechanism providing these advantages. This is likely due to the complexity of the thermal, mechanical, and electrical processes that may be involved with SPS. For example, the mere existence of spark plasma during sintering is one of the highly debated topics. However, it is now a generally accepted theory that the current causes joule heating at the inter-particle contact areas and the particles fuse upon the application of pressure [12].

Based on the apparent advantages, it is no wonder that the use of SPS for sintering nuclear fuel is now under investigation. The successful process-

ing of refractory materials has sparked interest in the applicability to fuel manufacturing. Significant work is in progress globally to understand the influence of individual parameters on fuel sintering behavior [13].

1.4 Thesis Objectives

The work done in this thesis aims to contribute to accident tolerant fuel research through the fabrication of silicide-containing uranium nitride fuel using the method of spark plasma sintering. Consequently, the findings should be relevant to future development of ATFs and should add to the presently growing knowledge on SPS behavior of nuclear fuel. The main objectives of the project were (i) to successfully fabricate UN-USi$_x$ nuclear fuel pellets using spark plasma sintering (SPS) and (ii) to characterize the resulting pellets.

Chapter 2

Characterization Methods

Several analysis tools were used for characterization of the alloys and pellets fabricated during this project. Priority was placed on evaluating the density, microstructure, and crystal structure of the resulting samples.

2.1   Density Measurement

The density was measured using Archimedes' principle, formulated after Archimedes of Syracuse (287-212 BC), which states that the upward buoyant force of a body immersed in a fluid is equal to the weight of the fluid displaced by the body. Legend has it that Archimedes discovered the physical law while trying to determine whether King Hiero II's crown was counterfeit. He allegedly immersed the crown and a piece of pure gold separately in water and compared the volume of displaced liquid from each. As a result, he was able to determine if the crown was pure gold by indirectly comparing the densities of the two objects [14].

Using Archimedes' principle with chloroform as the displacement fluid, the density was determined using the equation,

$$\rho_s = \frac{m_s}{m_s - m_{chlo}} * \rho_{chlo} \tag{2.1}$$

where ρ_s is the density of the object, m_s is the dry mass of the object, m_{chlo} is the mass of the object while immersed in chloroform, and ρ_{chlo} is the density of chloroform (1.483 g/cm^3). The setup used for density measurement is shown in Figure 2.1.

Figure 2.1: Setup used for density measurement.

2.2 Microstructure Characterization

Scanning electron microscopy (SEM) is an analysis tool that uses electron-sample interactions to characterize microstructure. The microstructure analysis was done with a XL-30 Field Emission ESEM microscope, shown in Figure 2.2. The microscope combines a high-brightness field emission gun source with a conventional electron column to bombard a sample with accelerated electrons. These electrons interact with the atoms in the sample, producing signals that are detected and interpreted. Each type of signal carries distinct information about the sample. For example, SEM imaging is typically done using a combination of secondary electron and backscatter electron detection. Secondary electrons provide information about the topography of the sample and backscatter electrons are used for rapid phase identification [15].

The samples were prepared for SEM analysis by mounting in bakelite, grinding with silicon carbon paper, and then diamond polishing for a smooth surface. The grinding and polishing were done with successively higher grits

and polishing pastes to make the sample surface as smooth as possible. After polishing, they were immersed in 95% ethanol and put into an ultrasonic bath for 20 minutes for cleaning.

Figure 2.2: XL-30 field emission ESEM microscope.

2.3 Crystal Structure Characterization

X-ray diffraction (XRD) is used for characterizing crystalline materials by providing information on phases, crystal orientations, and structural parameters present in the sample. A monochromatic beam is directed at a sample, and the intensities and angles of the diffracted beams are measured. Characteristic x-ray spectra are then used to analyze the material composition. XRD analysis was made with a Siemens D5000 X-ray diffractometer, using a Cu k-alpha target at a 40 mA current and 35 kV voltage. Powder samples were prepared by first grinding fine with a mortar and pestle, then smearing around 300 mg onto the flat surface of a sample holder.

Figure 2.3: Siemens D5000 x-ray diffractometer.

Electron backscatter diffraction (EBSD) is a SEM technique that is able to provide quantitative microstructural information about the crystallographic nature of materials, including the crystal structure, crystal orientation, and phase. EBSD is done experimentally by connecting an EBSD detector to a SEM, shown in Figure 2.4. The detector consists of a phosphor screen, compact lens, and CCD camera. For analysis, the sample is placed at a shallow angle incident to an electron beam. The diffracted electrons create an EBSD pattern, which is measured by the phosphor screen and converted into a light suitable for the CCD camera to record [16].
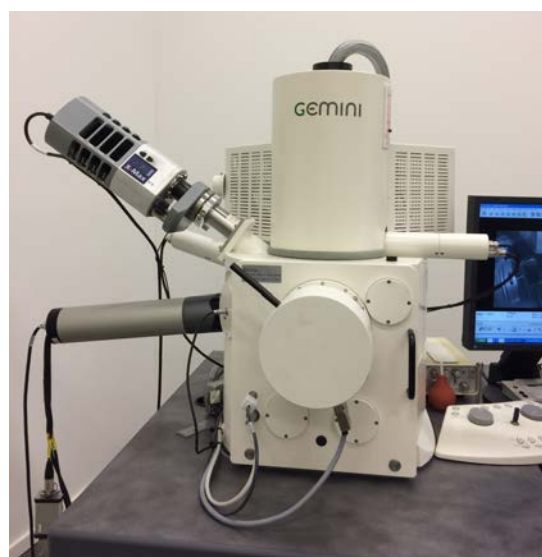
Figure 2.4: LEO 1530-FESEM equipped with EBSD detector.

2.4   Elemental Analysis

Oxygen and nitrogen analysis were done with a LECO TC-136 inert fusion gas instrument, pictured in Figure 2.5. Under a flow of helium gas, the instrument measures gases released from the sample after combustion. With these conditions, oxygen and carbon combine to form CO_2 and nitrogen is released as N_2 [17]. The analysis is destructive, but only requires around 30-60 mg of the sample to be used.

X-ray fluorescence (XRF) is another elemental analysis tool that was used. It measures the intensity of x-rays fluoresced by individual elements, giving the ability to quantify the amount of an element in a sample. The XRF analysis was done with a Thermo ARL 9800 instrument.

Energy dispersive spectroscopy (EDS) is a useful tool provided by the SEM, and uses backscatter electrons to determine what elements are present in the sample and their relative proportions. The EDS software quantifies elements by associating the energy level of x-rays with the elements and shell levels that generate them. However, there are some limitations on the ability of certain instruments to quantify the very light elements [18]. Therefore, specific quantification results should be taken as representative and not interpreted literally.

Figure 2.5: LECO TC-136 inert fusion gas instrument.

Chapter 3

Alloying Uranium and Silicon

Uranium metal has the extraordinary capability to be used as an abundant source of energy. Unfortunately, pure uranium also has poor mechanical properties and is chemically reactive. As a result, for nuclear fuel applications, uranium is typically alloyed with other materials in an attempt to improve these properties. There are a number of requirements to be met when considering which material to use as an alloy. First and foremost, the alloying material must be able to withstand the harsh environment of a nuclear reactor, including those conditions predicted in potential accident scenarios. This requires the material to have an acceptable ability to handle exposure to extreme heat and high irradiation. In addition, it is important to maintain a high uranium density in order to maximize fuel loading, thereby increasing the economical sustainability of nuclear power plants. Various other characteristics, such as compatibility with coolant and cladding materials, must also be taken into consideration. Since there is no perfect alloy, the choice is usually some compromise on the balance of these desired properties.

	Uranium	Silicon
Density, ρ	19.1 g/cm^3	2.33 g/cm^3
Melting Temperature, T_m	1132 °C	1414 °C
Boiling Temperature, T_b	4131°C	3265 °C
Thermal Conductivity, k	27.5 W/mK	149 W/mK
Thermal Expansion, α	13.9 μ/mK	2.6 μ/mK

Table 3.1: Properties of elemental uranium and silicon.

Table 3.1 contains some relevant properties of elemental uranium and silicon. In the case of the uranium-silicon alloy, multiple intermetallic compounds can be formed depending on the composition and alloying method used [19]. Therefore, alloying must be approached with careful analysis of the phase diagram and alloying technique.

3.1 U-Si Phase Diagram

The phase chosen for use in the composite fuel was U_3Si_2, due to the number of potentially favorable fuel performance properties. These properties include a high uranium density, a high thermal conductivity, and the possibility of performing well under irradiation compared to the other silicides [20]. Table 3.2 shows some properties of U_3Si_2 compared to uranium oxide. The high thermal conductivity compensates for the relatively low melting point of 1665 °C. The heat removal capability of this compound should improve fuel performance under accident conditions in a nuclear reactor.

	UO_2	U_3Si_2
Density	10.96 g/cm^3	12.2 g/cm^3
Uranium number density	2.45 x 10^{22}atom/cm^3	2.86 x 10^{22}atom/cm^3
Thermal conductivity	2.5-6 W/mK	21-38 W/mK
Melting point	2847 °C	1665 °C

Table 3.2: Selected properties for uranium oxide and U_3Si_2 fuels [21].

A phase diagram for the U-Si system is shown in Figure 3.1, which shows that U_3Si_2 will form at a composition of approximately 7.3 wt% Si. Due to the narrow range of homogeneity, it is essentially impossible to create an entirely homogenous alloy. Therefore, the silicides are always expected to contain more than one phase [22]. The amount of each phase present is directly related to alloy composition, homogeneity, and heat treatment. The presence of impurities complicates the situation further. Oxygen and source material impurities may interfere with the melting process and homogeneity of the final product. The theoretical densities for the six uranium silicide compounds are listed in Table 3.3. The formation of U_3Si should be avoided due to the alloy's poor irradiation performance at high burnup [5].
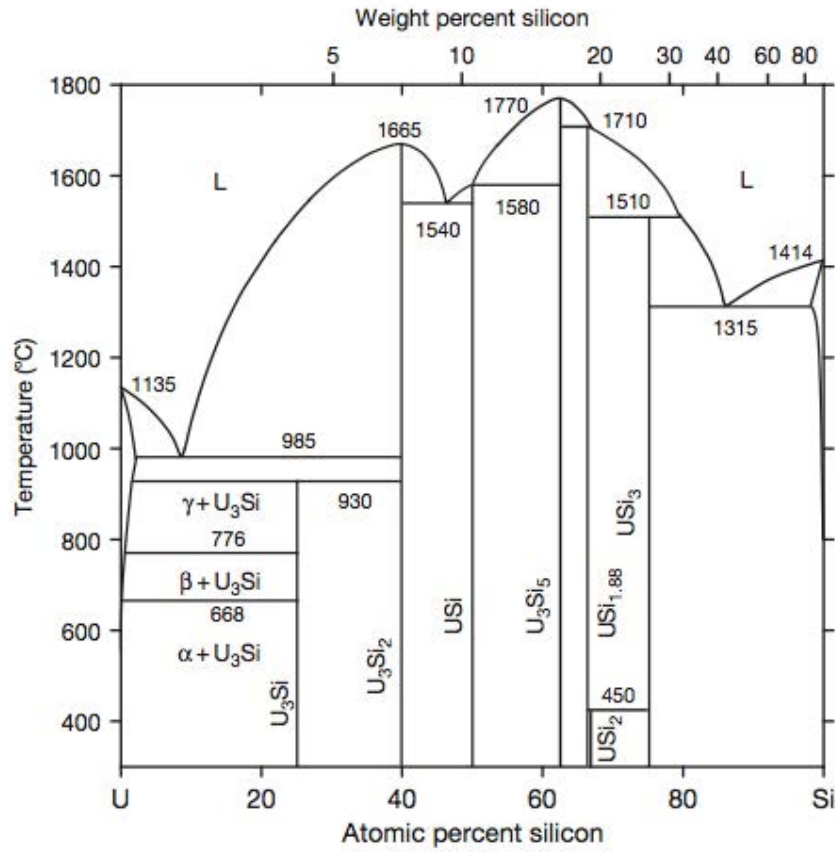
Figure 3.1: U-Si phase diagram [25].

Phase	Density
U_3Si	15.58 g/cm^3
U_3Si_2	12.20 g/cm^3
USi	10.40 g/cm^3
U_3Si_5	9.25 g/cm^3
USi_3	8.98 g/cm^3
USi_2	8.15 g/cm^3

Table 3.3: Theoretical densities for the uranium silicides [23].

3.2 Arc Melting

The raw materials used for the alloys were depleted uranium and 99.98% pure silicon, and the method chosen for alloying was triple arc melting. This decision was based on a literature review of alloying methods and past experience in the KTH fuels laboratory [24]. The triple arc melting furnace, shown in Figure 3.2, made the method of producing alloyed ingots quite simple. First, the composition was chosen based on analysis of the phase diagram and study of previous research in arc melting silicides [25]. The amount of silicon used was 7.5 wt% in order to obtain U_3Si_2. This value was higher than the one reported in the phase diagram, since previous studies have shown that using a slightly Si-rich composition suppresses the formation of uranium solid solution (U_{ss}) and U_3Si [22]. The method used for arc melting was:

1. Polish uranium pieces manually to remove oxide layer, then weigh.
2. Weight out desired amount of silicon.
3. Place materials in copper holder and place holder in arc melter.
4. Flush system with argon gas to create inert atmosphere.
5. Switch furnace on and melt materials together with the arcs until uniform button is made.
6. Flip button and re-melt four times to ensure homogeneity.

Figure 3.2: Triple arc melter used for melting alloys.

3.3 Resulting Alloys

Four silicides were created, with changes to composition made according to properties observed in the final products. These properties are summarized in Table 3.4. XRF analysis done on samples AUSi150224A and AUSi150224B showed resulting silicon contents of 7.04 wt% and 4.45 wt%, respectively. The extremely low silicon content observed in sample AUSi150224B was believed to occur due to unmelted silicon left in the copper hearth combined with a possible over melting of the alloy. The composition for the remaining two alloys was raised to 7.8 wt% Si, due to the slight silicon loss observed in sample AUSi150224A.

Sample	Si Content	Mass Loss	Final Mass	Density
AUSi150224A	7.67 wt%	44.0 mg	3.40 g	12.01 g/cm^3
AUSi150224B	7.50 wt%	272.0 mg	10.82 g	11.63 g/cm^3
AUSi150313A	7.80 wt%	2.0 mg	8.80 g	12.11 g/cm^3
AUSi150512A	7.80 wt%	3.0 mg	8.85 g	12.11 g/cm^3

Table 3.4: Properties of fabricated uranium silicide alloys.

EDS confirmed the bulk of the material to be U_3Si_2. SEM analysis on the samples showed a fairly homogenous material, with some localized impurities. The majority of impurities found were oxides and elemental uranium, examples of which can be seen in Figures 3.4, 3.5, and 3.6. The source of the oxides was most likely the raw uranium metal, which contained a thick oxide layer that was polished off to the best of ability. Furthermore, some elemental uranium was expected in the alloys because of the absence of heat treatment, which would have caused the uranium to react to form U_3Si at the peritectoid temperature of 925 °C [20]. Heat treatment was initially attempted on one alloy then abandoned after the furnace proved to have an unreliable atmosphere.

Secondary silicide phases, although expected to be present, were difficult to identify with SEM. For this reason, XRD analysis was also done for phase identification. Figure 3.7 shows the diffraction pattern observed for sample AUSi150512A, one of the alloys later mixed into the pellets. Peak identification showed mostly U_3Si_2 with the apparent presence of some USi, which was expected due to the slightly silicon rich composition used.

Figure 3.3: Alloyed sample AUSi150313A.
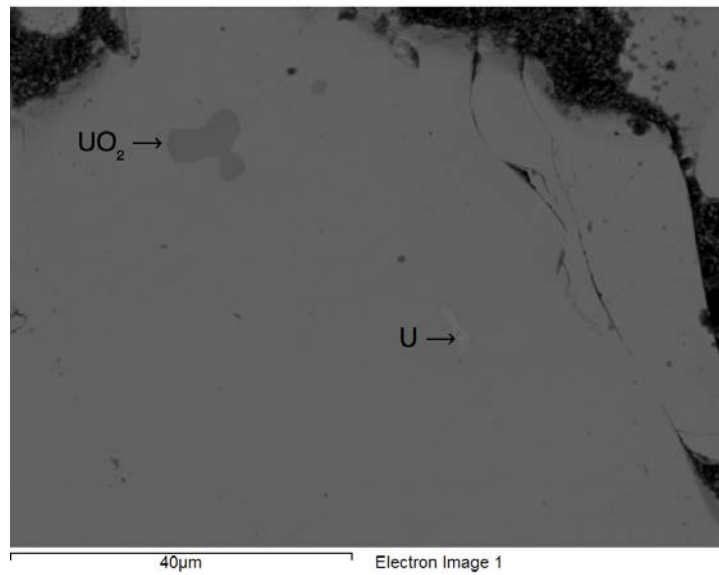
Figure 3.4: Impurities in alloyed sample AUSi150224B.

(a) BSE image of oxide.

(b) Elemental composition showing silicon (green), oxygen (red), and uranium (blue).
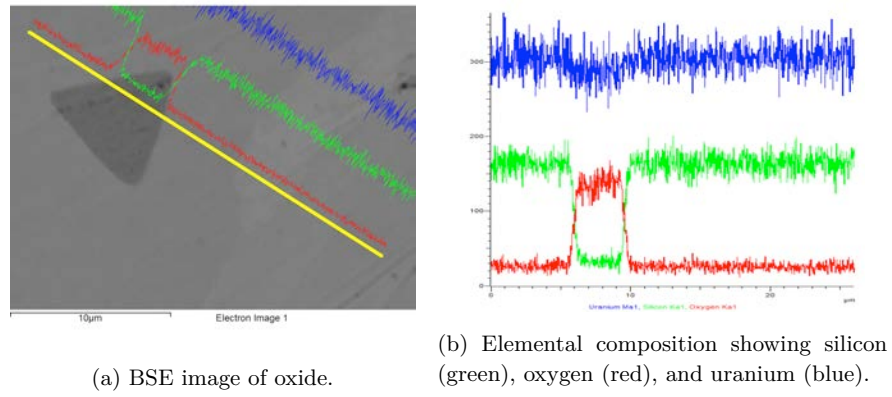
Figure 3.5: EDS line scan of AUSi150224B.
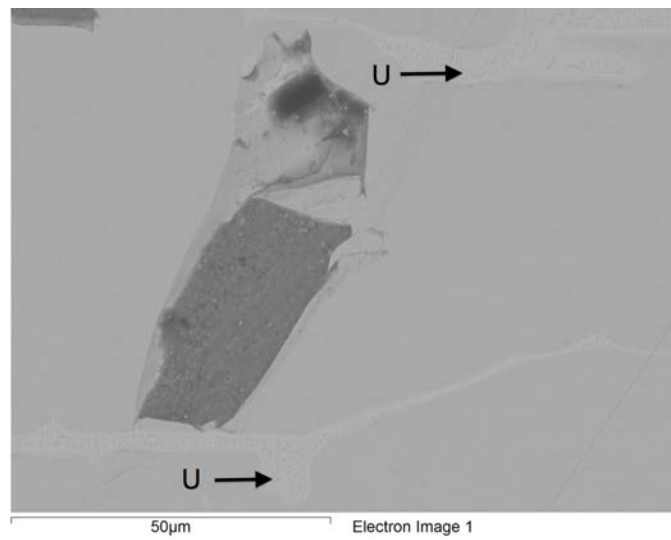
Figure 3.6: Unreacted uranium in alloyed sample AUSi150313A.
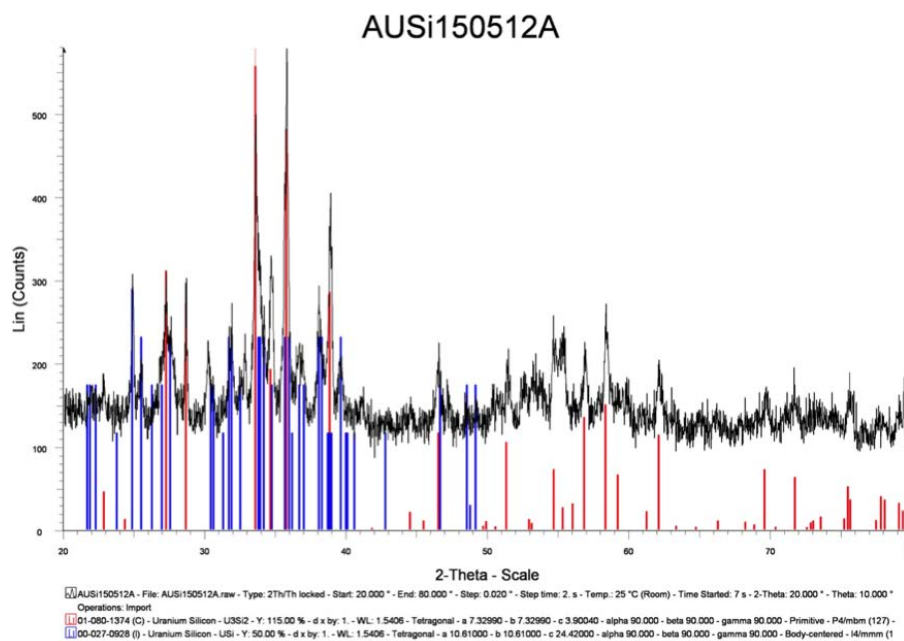
Figure 3.7: XRD pattern for alloyed sample AUSi150512A, showing peaks for U_3Si_2 (red) and USi (blue).

Chapter 4

Synthesizing Nitride Powder

Uranium nitride can formally exist in three different phases: uranium mononitride (UN), uranium sesquinitride (U_2N_3), and uranium dinitride (UN_2). The simplicity of the phase system allows for ease in fabrication of UN, especially the fact that the nitrogen rich phases decompose at high temperatures [26]. There are several popular methods used for synthesis of uranium mononitride, including carbothermic reduction of UO_2 and ammonolysis of UF_4. However, for this project, uranium mononitride was synthesized using a method called hydriding-nitriding, which has been under development at KTH. Whereas other methods of synthesis introduce impurities into the process, the major advantage of hydriding-nitriding is the ability to fabricate large batches of high purity nitride directly from metallic uranium.

4.1   Hydriding-Nitriding Method

For hydriding-nitriding, the synthesis of uranium mononitride is done by initiating three consecutive reactions inside of a furnace, shown in Figure4.1. First, metallic uranium is exposed to hydrogen gas at a temperature upwards of 225°C, which is the temperature required for uranium trihydride formation [27]. The temperature is ramped up to 325°C then taken down and held at 225°C for 2.5 hours, or until the reaction reaches completion. Under these conditions, uranium trihydride is formed according to the following reaction:

$$2U + 3H_2 \longrightarrow 2UH_3 \qquad\qquad \Delta H_r^\circ = -254 \text{ kJ/mol} \qquad (4.1)$$

The difference in specific volume causes the UH_3 to spall off as a fine

powder [28]. The powder remains in the reaction chamber to limit exposure to oxygen, since it is highly pyrophoric [29]. Nitriding can be done immediately afterwards by exposing the uranium hydride to nitrogen gas, with the reaction starting around 250°C. The N_2 is introduced at an ascending temperature ramp until reaching 500°C, triggering the reaction:

$$2UH_3 + 1.5N_2 \longrightarrow U_2N_3 \qquad\qquad \Delta H_r^\circ = -1013 \text{ kJ/mol} \quad (4.2)$$

Lastly, denitriding is done by exposing the sesquinitride to temperatures above 1150°C, causing the formation of a mononitride from the reaction:

$$U_2N_3 \longrightarrow UN + 0.5N_2 \qquad\qquad \Delta H_r^\circ = 1879 \text{ kJ/mol} \quad (4.3)$$

The nitride powder is then cooled to room temperature with a continuous flow of argon gas and carefully transferred to a glove box to prevent oxidation.

4.2 Powder Synthesis

The synthesis was done in a quartz tube which was placed inside of a furnace, shown in Figure 4.1. The quartz tube was loaded with a 62.0 g piece of uranium metal, sealed, and insulated. The progression of individual reactions was determined by measuring the gas flow difference,

$$dF = F_{out} - F_{in} \qquad\qquad (4.4)$$
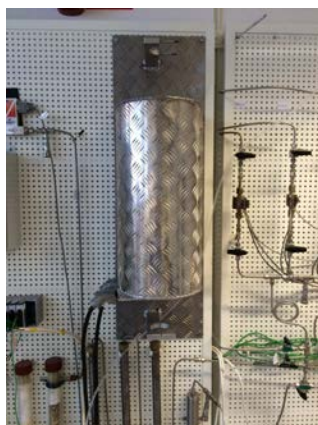
Figure 4.1: Furnace used for nitride powder synthesis.

For hydriding, the gas flow was set to 0.5 L/min H_2 and 0.4 L/min Ar. The temperature was taken to 325 °C then lowered to 225 °C at a rate of 5 °C/min, since hydrogen uptake was found to increase during cooling [28]. Figure 4.2 shows the flow difference as a function of temperature during hydriding. The initial peak in this graph is from initiation of gas flow, but the remaining ones represent the progression of the reaction. The time required for the reaction to reach completion was 2.5 hours.

Nitriding is done by changing the gas flow to 0.5 L/min N_2 and ramping the temperature up from 225 °C to 500 °C at a rate of 10 °C/min. This reaction is highly exothermic, causing the temperature to increase faster than the ramp rate. There is also an outgassing of hydrogen before the uptake of nitrogen. These effects are demonstrated in Figure 4.3, which also shows that the reaction took around 1 hour for completion.
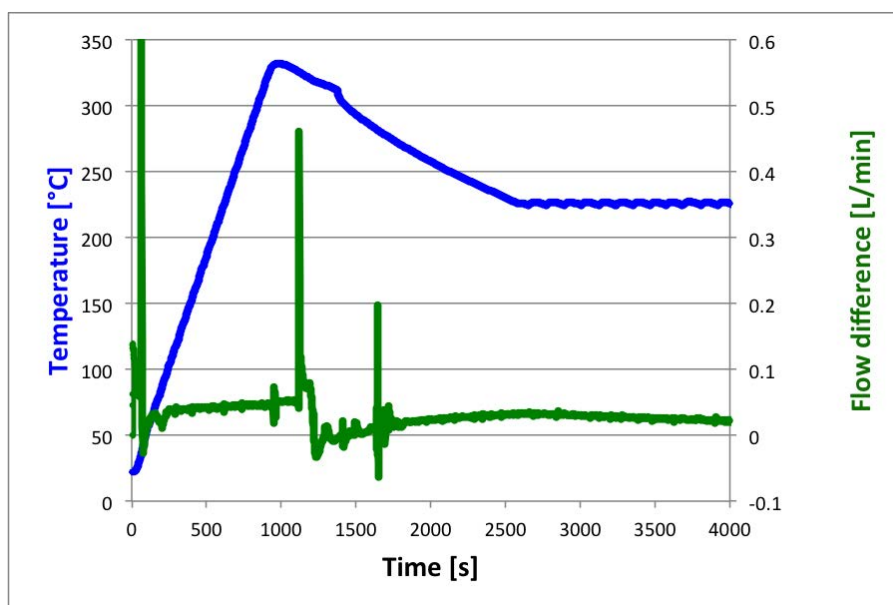
Figure 4.2: Gas flow difference and temperature during hydriding.
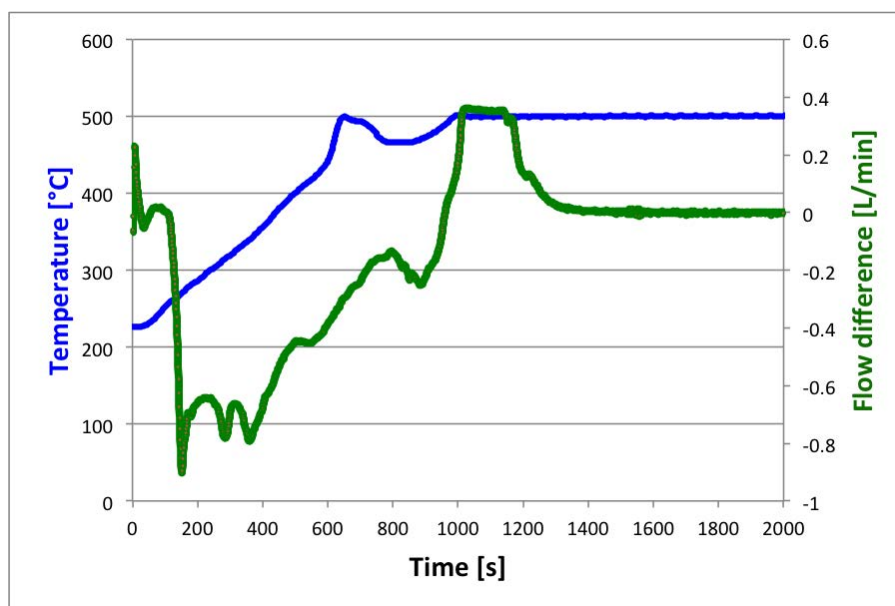
Figure 4.3: Gas flow difference and temperature during nitriding.

Denitriding is performed at high temperature and under an argon atmosphere. The temperature was increased to $1150\,°C$ and gas flow was switched to 0.5 L/min Ar. The temperature is unfortunately limited by the performance of the quartz tube, meaning the reaction will proceed more slowly. The reaction is considered complete when there is no longer an outflow of nitrogen detected, which can take upwards of 5 hours. In this case, the reaction was even held some time after the zero-flow point was reached to ensure that the reaction had reached completion. The graph of the flow difference for the denitriding step is shown in Figure 4.4; the reaction was actually held for 6 hours. The resulting powder, shown in Figure 4.5, was measured to be 5.33 wt% nitrogen and 0.11 wt% oxygen.
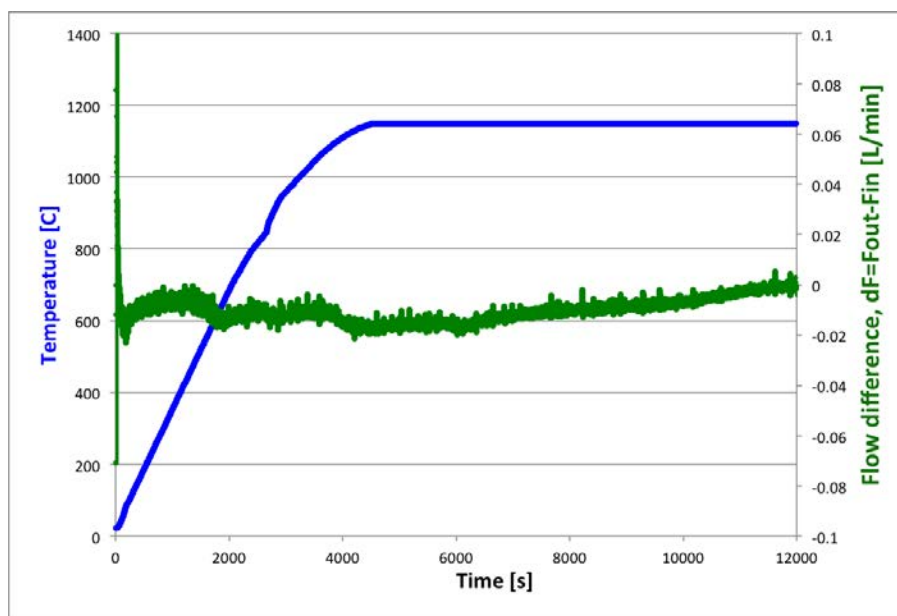
Figure 4.4: Gas flow difference and temperature during denitriding.

Figure 4.5: Resulting uranium nitride powder.

Chapter 5

Fuel Pellets - Composition Optimization

Initially, four pellets with varied compositions were made in order to test the sintering behavior of the materials. The initial goal with this approach was to determine the maximum amount of silicide that could be added to the fuel and successfully sintered. After sintering, a thorough characterization and analysis was done on the resulting pellets.

5.1   Pellet Preparation

Powder preparation was done inside of a glove box, shown in Figure 5.1. First, the uranium silicide was ground into a powder using a mortar and pestle. The silicide was brittle, so grinding was done with ease. Next, four different compositions were mixed with uranium nitride powder in proportions of 5%, 10%, 20%, and 25 wt% U_3Si_2. Due to the lack of access to a proper milling device, the powders had to be manually mixed.

Figure 5.1: Glove box used for mixing powders.

5.2 Sintering

Spark Plasma Sintering was done with a DrSinter SPS-5.40MK-VI (Figure 5.2), which was enclosed in a glove box. For each pellet, approximately 5.0 g of powder was loaded into a graphite foil, which was enclosed in a graphite die of 12 mm diameter. The sintering parameters were chosen based on past experience sintering nitride pellets at KTH [30]. The parameters were fixed for each pellet at a pressing pressure of 155 MPa, sintering temperature of $1450\,^{\circ}$C, and holding time of 3 minutes. Figure 5.3 shows the parameter profile during sintering of the four pellets. The z-axis displacement curve, which measures the motion of the punch, reflects the densification of the pellet. The similarity of this curve between the pellets therefore indicates that they should have comparable densities.

Figure 5.2: DrSinter SPS-5.40MK-VI used for sintering.
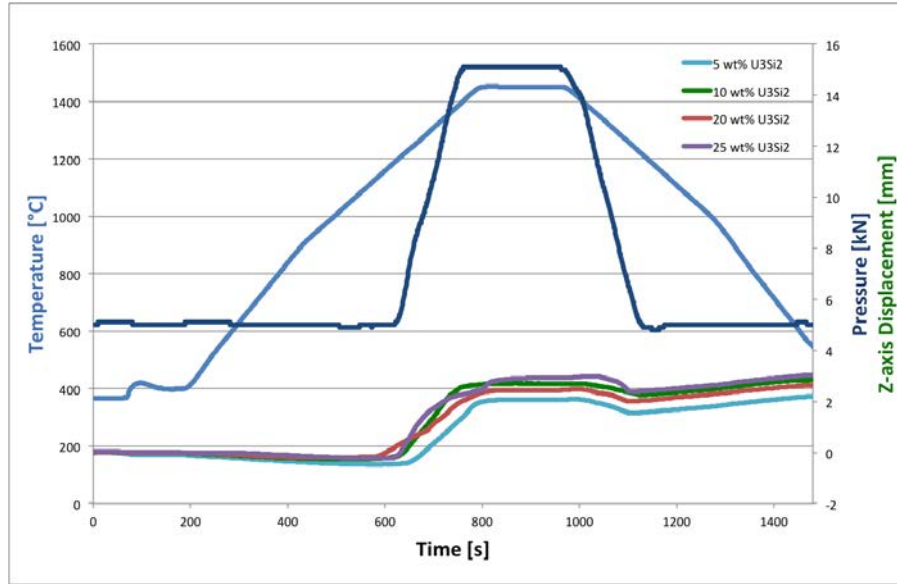
Figure 5.3: SPS parameter profile for pellets with varied silicide composition.

5.3   Resulting Pellets

The pellets were polished to remove the layer of graphite, which is formed because the graphite foil fuses to the pellet surface during sintering. Figure 5.4a and Figure 5.4b are photos of a pellet before and after polish, respectively. As expected, the densities of the pellets were very similar, indicating that the high pressing pressure had a significant impact on densification. The densities are listed in Table 5.1.

When removing the pellets after sintering, the higher silicide composition pellets (20 wt% and 25 wt%) deposited some melted metal onto the surface of the graphite die. The metal was radioactive, which leads to the conclusion that some liquid uranium phase, or perhaps even uranium silicide, had melted during sintering. The result of this finding was to limit the composition to 10 wt% for the remainder of the sintering experiments.

(a) Before polish.

(b) After polish.

Figure 5.4: Pellet SUNUSi150423A1 (5% U_3Si_2).

Pellet	Composition	Density
SUNUSi150423A1	5 wt% U_3Si_2	13.92 g/cm^3
SUNUSi150423A2	10 wt% U_3Si_2	13.72 g/cm^3
SUNUSi150423A3	20 wt% U_3Si_2	13.72 g/cm^3
SUNUSi150423A4	25 wt% U_3Si_2	13.82 g/cm^3

Table 5.1: Densities for pellets of varied silicide composition.

SEM analysis of the pellets revealed a distinct dark intergranular phase, pictured in Figure 5.5. The initial observation was the similarity of microstructure to that seen in liquid phase sintering, which exhibits a distinguishable wetting behavior of a secondary phase on the grain boundaries of solid particles. The possibility that liquid phase sintering occurred was supported by the melt found on the graphite dies from the higher silicide pellets.

The observed intergranular phase was originally assumed to be U_3Si_2, but was discovered to be silicon-rich in comparison. In fact, EDS analysis gave an average composition of 32 at% U, 54 at% Si, and 14 at% N. The presence of nitrogen and the corresponding possibility of having a ternary phase was very unexpected. However, the same characteristic phase was found in all four pellets in varying proportions.

(a) SUNUSi150423A3 (20 wt% U_3Si_2). (b) SUNUSi150423A4 (25 wt% U_3Si_2).
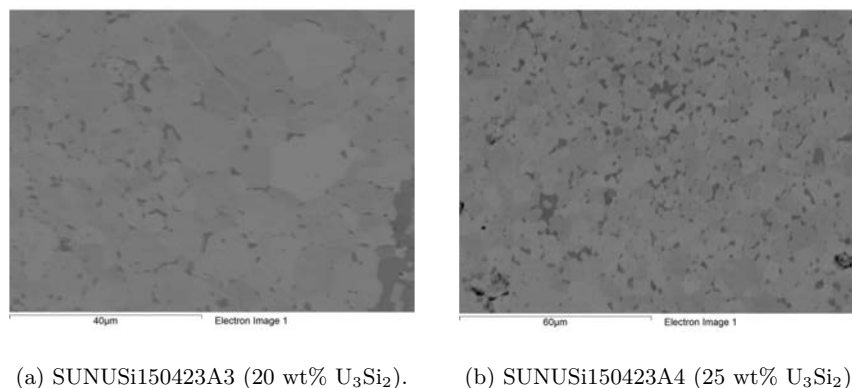
Figure 5.5: BSE images of observed intergranular phase.

The absence of milling actually gave some hints to the formation of this unidentified phase. The particle size difference meant that large inclusions of uranium silicide existed within the bulk of uranium nitride. Figure 5.6 and Figure 5.7 are two examples of these structures, all of which had the same general characteristics. First, the dark outer material showed the same characteristics as the previously introduced intergranular phase, with an averaged composition of 32 at% U, 55 at% Si, and 13 at% N. However, the inner material was uranium-rich, with an averaged composition of 60 at% U, 35 at% Si, and 5 at% N. This phase more closely resembled the original U_3Si_2, with the major difference being the apparent addition of nitrogen.
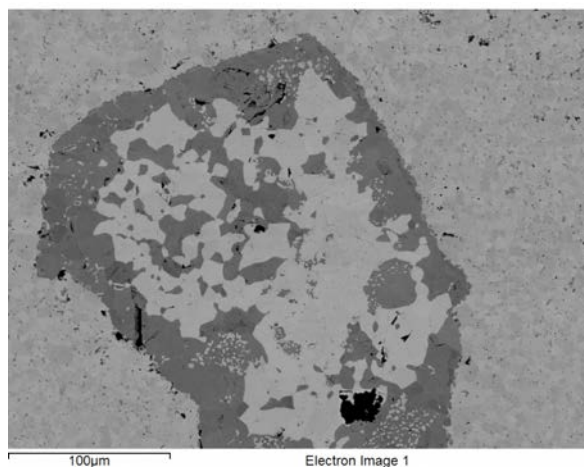
Figure 5.6: Silicide inclusion from pellet SUNUSi150423A2 (10% U_3Si_2).
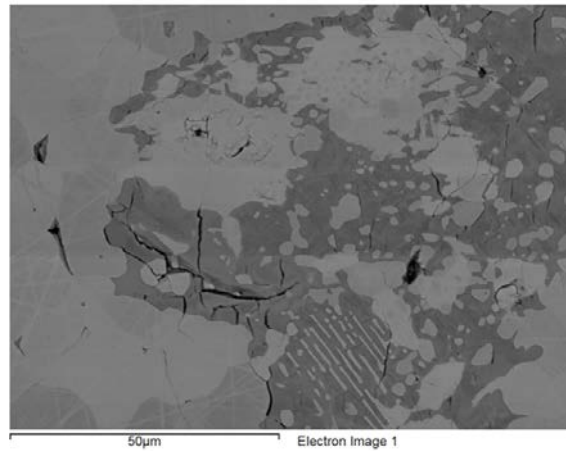
Figure 5.7: Silicide inclusion from pellet SUNUSi150423A1 (5% U_3Si_2).

There were also a few large inclusions of U_3Si_2 found, an example of which is shown in Figure 5.8. However, these unreacted silicide inclusions were difficult to locate. Figure 5.9 conveniently shows a U_3Si_2 inclusion directly adjacent to the unidentified silicon-rich phase. A line scan shows a clear difference in silicon and uranium content between the two phases (Figure 5.10).
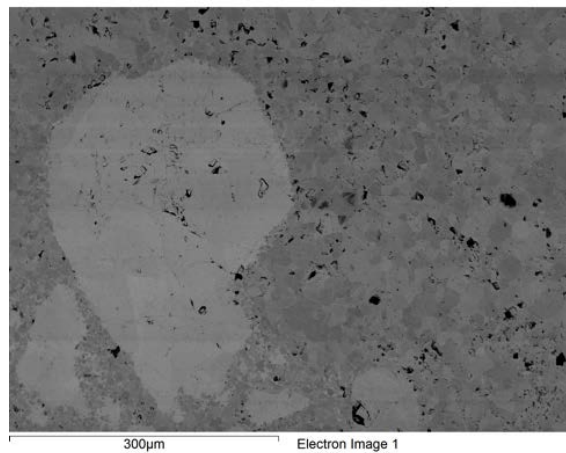
Figure 5.8: U_3Si_2 inclusion from pellet SUNUSi150423A4 (25% U_3Si_2).
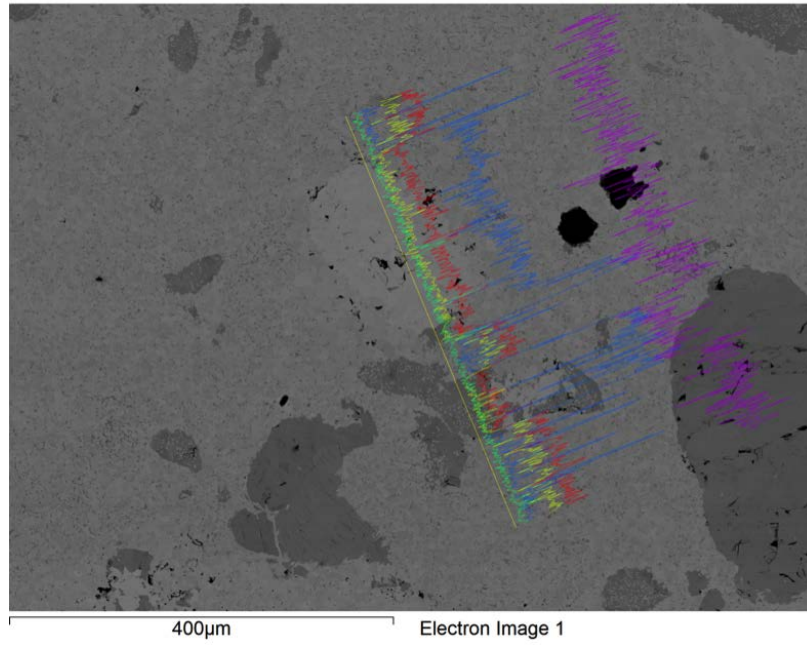
Figure 5.9: Adjacent silicide inclusions from pellet SUNUSi150423A2 (10% U_3Si_2).

(a) Silicon content.

(b) Uranium content.
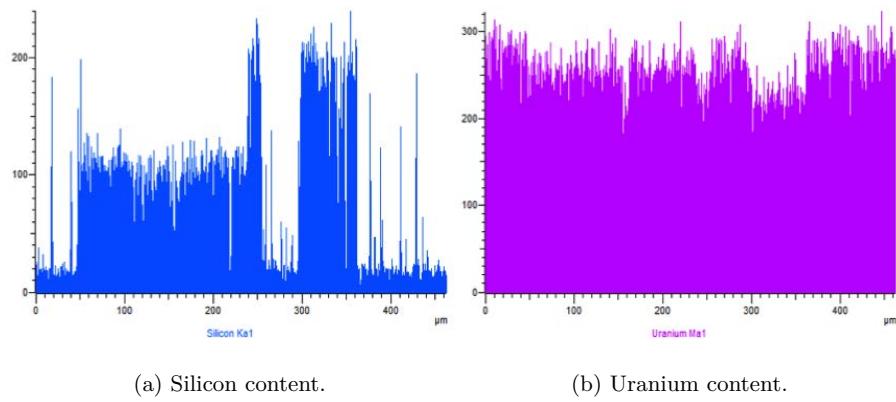
Figure 5.10: Line scan of adjacent silicide inclusions from pellet SUNUSi150423A2 (10% U_3Si_2).

Another characteristic worth mentioning is that uranium nitride particles seemed to have migrated into the inclusions (Figure 5.11). This attribute further supports the idea that liquid phase sintering occurred, and suggests that the solid uranium nitride has dissolved into the liquid uranium silicide phase.

Figure 5.12 shows the XRD patterns for the 10 wt% U_3Si_2 pellet before and after sintering. The new peaks in the post-sintering spectrum suggest the formation of a new phase during sintering. However, these peaks did not seem to match the crystallographic data for any known phases.

In summary, the analysis of these four pellets suggested that some sort of chemical reaction occurred during sintering, transforming the U_3Si_2 into a possible ternary U-N-Si phase. As a consequence, this observation took the project in a new direction with an additional objective - attempt to identify when this phase transition occurs.
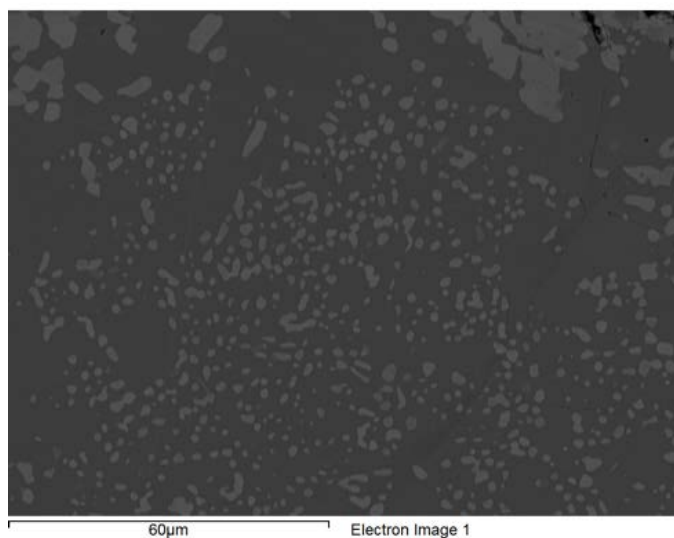
Figure 5.11: UN particles sequestered inside of silicon-rich phase.
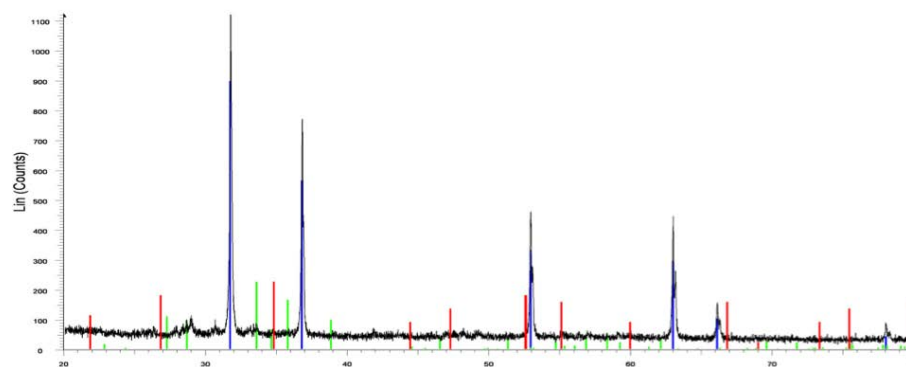
(a) Powder before sintering.
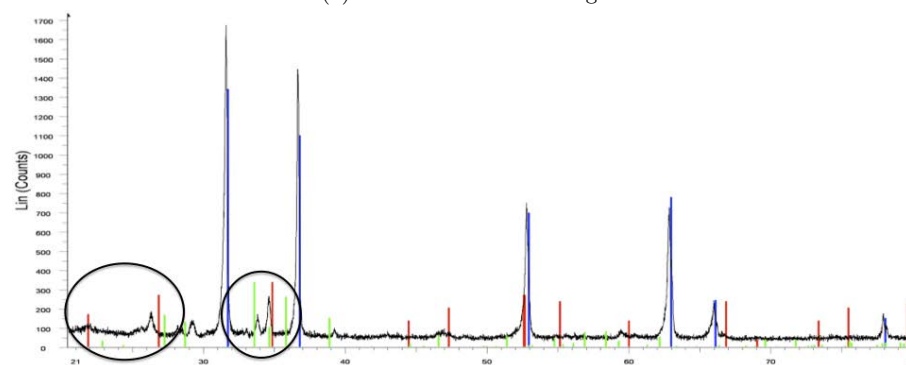
(b) Pellet after sintering.

Figure 5.12: XRD patterns for sample SUNUSi150423A2 (10 wt% U_3Si_2) before and after sintering.

Chapter 6

Fuel Pellets - Temperature Optimization

After the discovery of the unidentified phase in all four of the previously made pellets, the project was extended to try and identify the temperature at which the phase change occurred. In order to do this, four more pellets were sintered at varying temperatures: $1200\,°C$, $1300\,°C$, $1400\,°C$, and $1500\,°C$.

6.1   Pellet Preparation

The process for pellet preparation was altered with the intent of creating a more similar particle size between the nitride and silicide, since previously the silicide particle size was much larger due to the absence of milling. In order to do this, the nitride powder was pre-compacted. The powder was loaded with 7.0 g batches into a 10 mm die and pressed with 2 tons using a MTI desk-top electromotion presser (Figure 6.1). The uranium silicide was ground with a mortar and pestle, same as before. Afterwards, the nitride and silicide were manually mixed with a fixed composition of 10 wt% U_3Si_2.

6.2   Sintering

Temperature aside, the sintering parameters were fixed at a pressing pressure of 55 MPa and holding time of 3 minutes. The mass was also fixed at approximately 5.0 g for each pellet. Figure 6.2 shows the SPS parameter profile with temperature and z-axis displacement curves. The displacement curves suggest increased densification with increased sintering temperature, a feature which is confirmed later with density measurements.

Figure 6.1: MTI desk-top electromotion presser.
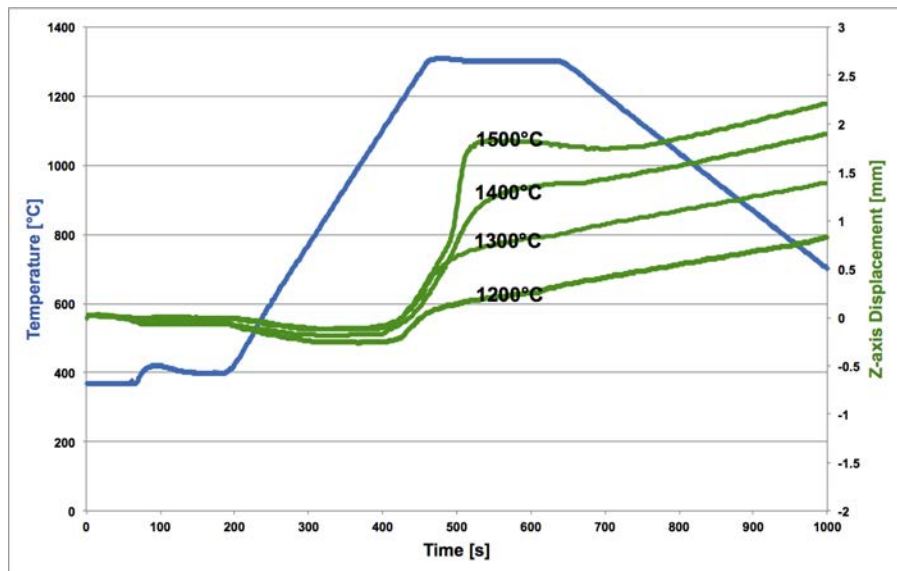
Figure 6.2: SPS Parameter profile for pellets with varied sintering temperature.

6.3   Resulting Pellets

The densification curves accurately reflected the difference in density, which increased as sintering temperature increased. Since the pressing pressure was kept constant at a relatively low value, the temperature was clearly the driving mechanism for sintering. The resulting pellets are shown in Figure 6.3 and their densities are listed in Table 5.1. Theoretical density was not addressed, since at this point the phases resulting from sintering were not fully defined.

Sample	Temperature	Density
SUNUSi150611A1	1200 °C	9.08 g/cm^3
SUNUSi150611A2	1300 °C	10.80 g/cm^3
SUNUSi150611A3	1400 °C	12.66 g/cm^3
SUNUSi150611A4	1500 °C	13.78 g/cm^3

Table 6.1: Density for pellets of varied sintering temperature.

(a) SUNUSi150611A1 (1200 °C).   (b) SUNUSi150611A2 (1300 °C).

(c) SUNUSi150611A3 (1400 °C).   (d) SUNUSi150611A4 (1500 °C).

Figure 6.3: Photo of the pellets from least dense (a) to most dense (b).

First, a thorough SEM analysis was done on all of the pellets to determine which phases could be observed. The first observation was the presence of distinct inclusions of U_3Si_2 in the lower temperature pellets (1200 °C and 1300 °C), shown in Figure 6.4. These inclusions had a very similar shade compared to uranium nitride, and were difficult to find if not for small areas of a darker silicon-rich phase located in the center. It is important to mention that there was no nitrogen dissolved into either of these phases.

EBSD analysis was done on the 1300 °C pellet, and was able to confirm the presence of U_3Si_2 located in some intergranular regions of the microstructure, pictured in Figure 6.5. Essentially, the U_3Si_2 is located exactly where the new phase is found in the higher temperature pellets. This indicates that the phase transformation into a ternary phase is temperature dependent and involves the exchange of uranium and nitrogen with the bulk uranium nitride material. More specifically, the atomic composition of the ternary phase would suggest that the U_3Si_2 loses uranium and gains nitrogen.
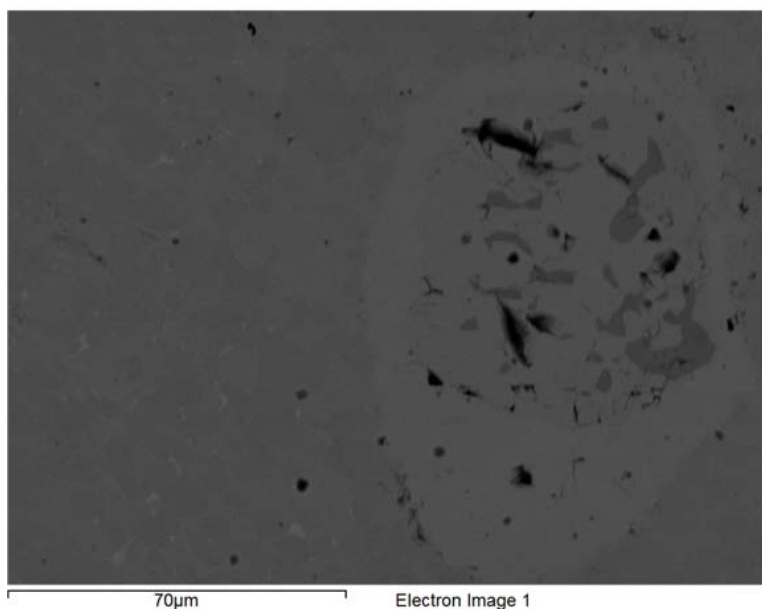
Figure 6.4: BSE image of a U_3Si_2 inclusion found in SUNUSi150611A2 (1300 °C) pellet.

(a) BSE image.   (b) SE image.
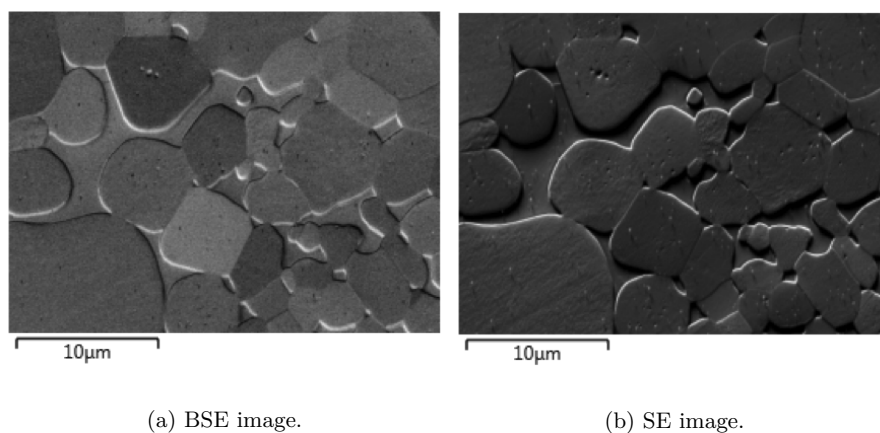
Figure 6.5: EBSD images of SUNUSi150611A2 (1300 °C) pellet microstructure, with intergranular U_3Si_2.

The same unidentified silicon-rich ternary phase was found in all of the pellets, having a very similar appearance to what was previously seen (Figure 6.6). However, it was much less abundant in the 1200 °C and 1300 °C pellets. EDS characterized the phase again as containing nitrogen, with an average composition of 44 at% U, 47 at% Si, and 9 at% N. Figure 6.7 shows an example of the phase located between the grains in the bulk and Figure 6.8 shows a large inclusion. The 1400 °C sample was taken to do EBSD analysis to try and identify this phase.

(a) SUNUSi150611A3 (1400 °C).   (b) SUNUSi150611A4 (1500 °C).
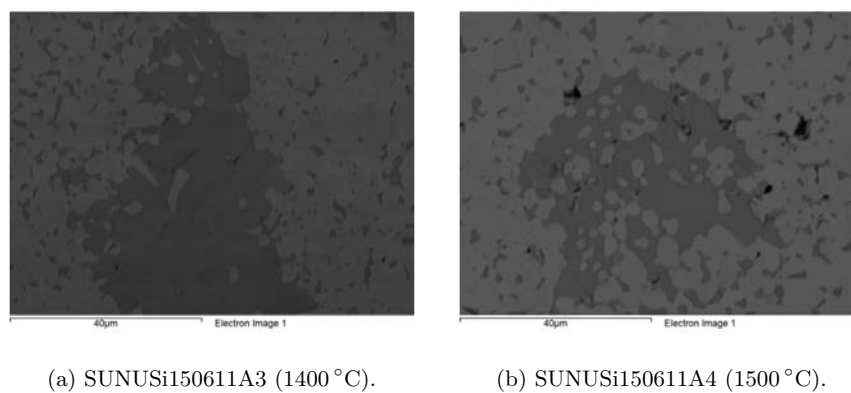
Figure 6.6: BSE images of silicon-rich phase found in higher temperature pellets.
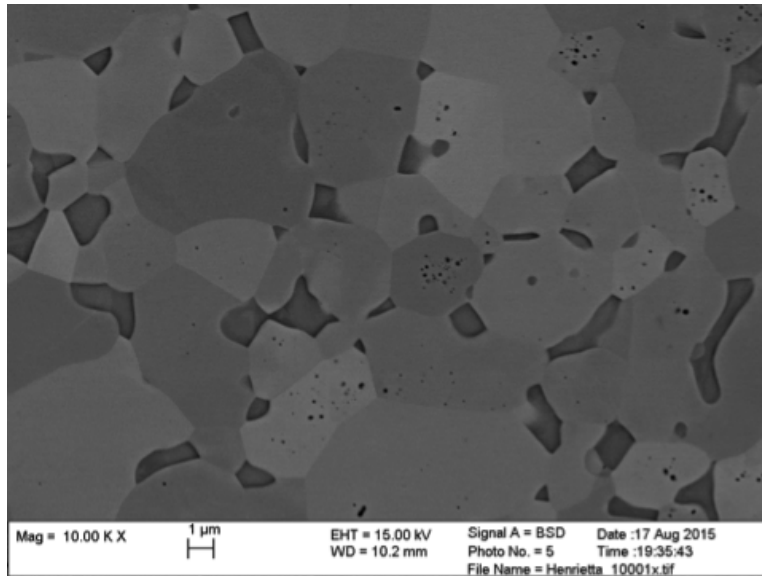
Figure 6.7: BSE image of dark intergranular phase found in SUNUSi150611A3 (1400 °C) pellet.
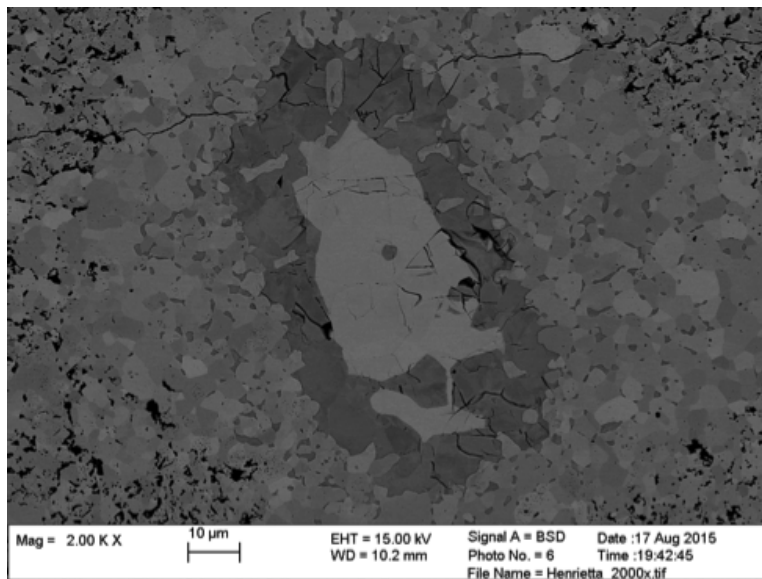
Figure 6.8: BSE image of silicide inclusion found in SUNUSi150611A3 (1400 °C) pellet.

EBSD, while able to produce beautiful pictures of the microstructure topography (Figure 6.9), was unfortunately unable to match the suspected ternary phase to any known phase patterns. This was not exactly surprising, since the ternary phase system for U-N-Si has not yet been defined. These results are still useful as they confirm that this is not a binary phase of U-Si and reiterate the fact that nitrogen must be diffusing. This nitrogen diffusion is clearly temperature dependent, since an increase in the ternary phase is seen in the higher temperature pellets.
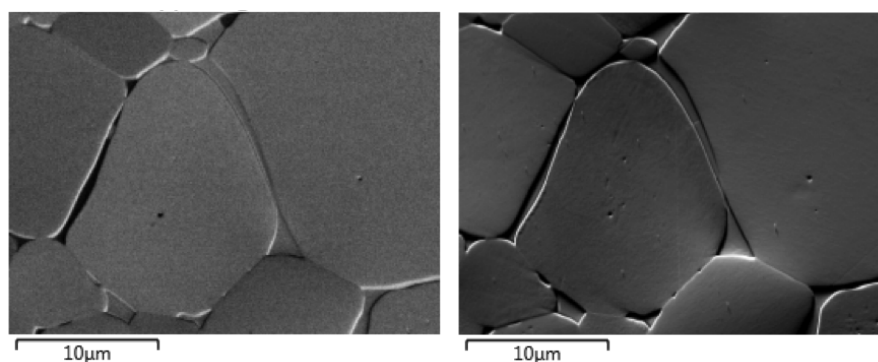
(a) BSE image.   (b) SE image.

Figure 6.9: EBSD image of dark intergranular phase found in SUNUSi150611A3 (1400 °C) pellet.

One interesting difference in the microstructure of the 1200 °C and 1300 °C pellets was a very uranium-rich phase located in the intergranular regions, shown as a bright phase in Figure 6.10. This phase was mostly observed in the most dense regions of the pellet surface, highlighting the heterogeneity of the pellets. EDS characterized the phase as 97.7 at% U, 2.0 at% Si and 0.3 at% N, which is very close to pure uranium metal. Figure 6.11 is a line scan showing the decrease in nitrogen and increase in uranium in this region. It is worth mentioning here that the line scan graph is purely representative of the relative compositional changes, since the quantification cannot be trusted. This intergranular uranium could have its origins in the silicide or the nitride. However, since the silicide is essentially losing uranium while forming the new ternary phase, there is a high chance that this uranium is a byproduct of that reaction.
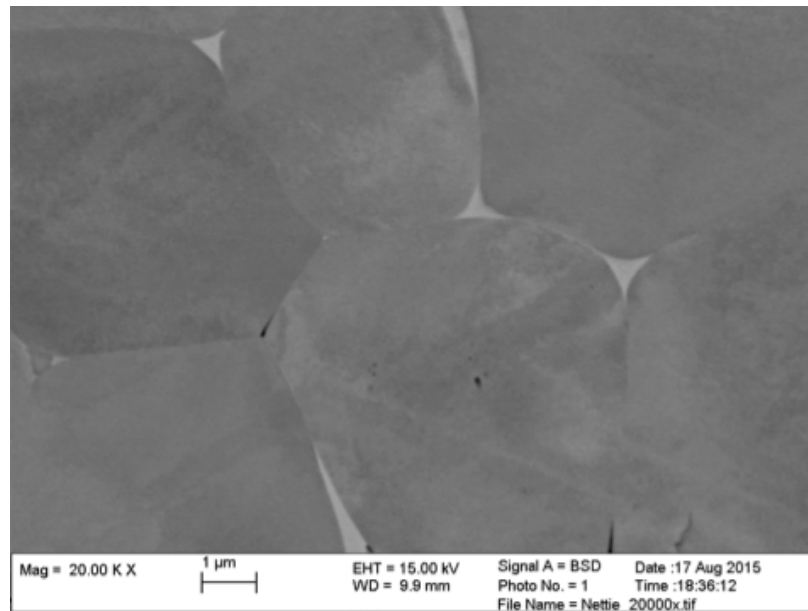
Figure 6.10: Light intergranular phase found in SUNUSi150611A2 (1300 °C) pellet.
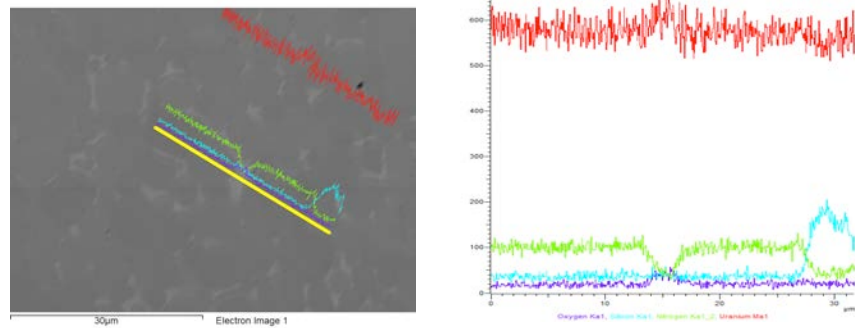
(a) BSE image of area containing light inter-granular phase.

(b) Line scan results showing nitrogen (green), uranium (red), and silicon (blue), and oxygen (purple).

Figure 6.11: EDS line scan of SUNUSi150611A2 (1300 °C).

Chapter 7

Conclusions

The fabrication work done during the course of this project has brought about results that are immediately relevant to the development of UN-USi$_x$ fuels. On the basis of these results and corresponding analysis, some general remarks can be made to summarize the observed sintering behavior of uranium nitride with uranium silicide.

First, the formation of a probable ternary U-N-Si phase during sintering is observed. The emergence of a new phase in the resulting fuel is generally unacceptable, since it can change the neutronics, irradiation behavior, mechanical, and thermal properties of the fuel during reactor operation. For instance, the existence of intergranular uranium metal found in the low temperature pellets would be detrimental to fuel performance. It is well known that uranium metal has a low melting temperature and poor swelling performance. The problem with having an unidentified phase in the fuel is that the performance has not yet been analyzed. Nuclear fuel must be accurately characterized before considering use in a reactor in order to predict behavior during normal operation and accidental conditions.

Some suggestions can be made as far as attempting to avoid the formation of these undesired phases. The uranium metal could possibly be avoided by using a uranium silicide with a lower U/Si ratio, such as U$_3$Si$_5$. However, this may have no effect the diffusion of nitrogen into this phase. It appears that the U-N-Si phase is formed at some threshold temperature, since the amount observed in the pellets increases with increasing temperature. If this is true, then the formation of the phase can easily be avoided by sintering below this threshold temperature. If the required sintering temperature is so low that it prevents achieving a high-density fuel with conventional sintering, then SPS may turn out to be a beneficial method of sintering. It is very likely that SPS could produce a highly dense pellet sintering at

an even lower temperature than 1200 °C. Of course, the pressing pressure would have to be simultaneously increased to a substantially higher value in order to achieve a fully dense material. Nevertheless, even if UN-U_3Si_2 fuel is successfully manufactured, the possibility of a phase transformation occurring at high temperatures within a reactor is still a remaining problem. One goal of accident tolerance is that the fuel integrity should be maintained as long as possible under accidental conditions.

As far as characterizing the ternary phase, it may not be possible until the correct thermodynamic data on the ternary U-N-Si system has been properly defined. Once the thermal analysis experiments have been completed to collect the necessary data, phase identification can be done and thermodynamic modeling can predict the behavior of the system. Currently, the diffusion mechanism causing the phase transformation can only be speculated and verification requires that the experiments be coupled with modeling. Still, phase identification involves a significant amount of work so this process could take a considerable amount of time.

The results also reveal some issues with using SPS to sinter nuclear fuel without proper understanding of the mechanism involved in sintering. For instance, one problem is the accuracy of temperature measurements during sintering. It is well understood that localized temperatures are not identical to the surface temperature recorded by the pyrometer. The temperature induced by the electrical current at the grain boundaries is not clearly defined, but is suspected to be much higher than the global temperature. In fact, depending on thermal conductivity of the material, even the global temperature can vary across the pellet by as much as 100 °C [31]. This temperature discrepancy requires redefining the proper temperature for sintering materials. For example, the uranium silicide in these pellets appeared to have melted at a surface temperature as low as 1200 °C, even though the melting temperature is 1650 °C. This is indicative of the need to evaluate the point at which liquid phase sintering occurs for individual materials while using SPS.

This raises another concern that is associated with using SPS to sinter composites, which is the distribution of current in two different materials. Experiments with SPS have shown that the presence of an electrically conductive material aids with the sintering process. Although this can be an advantage, it can also cause the sintered material to be highly heterogeneous. The current may have preference to flow through one material over another and cause vast differences in local temperatures and sintering rates. On the other hand, this could be beneficial if the desire to is to perform liquid phase sintering with a more electrically conductive phase.

In summary, an accident tolerant UN-USi composite may still be a feasible fuel concept, but cannot be recommended for use in a reactor until these issues are addressed and the phase transformation is fully characterized. High priority should be placed on thermodynamically evaluating the U-N-Si ternary system in order to predict fuel behavior at elevated temperatures. In the same way, spark plasma sintering has a number of obstacles that must be overcome before it becomes a practical method to manufacture nuclear fuel. However, the increased interest in the scientific community is largely closing the gap of knowledge, so it is not unreasonable to think that one day the method could be widely used.

Bibliography

[1] Zinkle, S.J., Terrani, K.A., Gehin, J.C., Ott, L.J., Snead, L.L. (2014). Accident Tolerant Fuels for LWRs: A perspective. Journal of Nuclear Materials, 448, 374-379.

[2] Pukari, Merja. (2013) *Experimental and theoretical studies of nitride fuels.* (Doctoral dissertation, KTH Royal Institute of Technology, Stockholm, Sweden).

[3] Sunder, S., Miller, N.H. (1998). XPS and XRD studies of corrosion of uranium nitride by water. Journal of alloys and compounds, 271, 568-572.

[4] Snelgrove, J.L., Hofman, G.L., Trybus, C.L., Wiencek, T.C. (1996). Development of very high density fuels by the RERTR program. Argonne National Laboratory, Argonne, Illinois, USA.

[5] Ugajin, M., Akabori, M., Itoh, A., Ooka, N., Nakakura, Y. (1997). Behavior of neutron-irradiated U_3Si. Journal of Nuclear Materials, 248, 204-208.

[6] Lessing, Paul A. (2012). Oxidation Protection of Uranium Nitride Fuel Using Liquid Phase Sintering. Idaho National Laboratory, Idaho Falls, Idaho, USA.

[7] Miranzo, P., Gonzalez-Julian, J., Osendi, M.I., Belmonte, M. (2011). Enhanced particle rearrangement during liquid phase spark plasma sintering of silicon nitride-based ceramics. Ceramics International,37(1), 159-166.

[8] Taylor, G.F. (1933). Apparatus for Making Hard Metal Compositions. US Patent No. 1,896,854.

[9] Munir, Z.A., Anselmi-Tamburini, U., Ohyanagi, M. (2006). The effect of electric field and pressure on the synthesis and consolidation of

materials: A review of the spark plasma sintering method. Journal of Material Science, 41, 763-777.

[10] Guyot, P., Rat, V., Coudert, J.F., Jay, F., Maitre, A., Pradeilles, N. (2012). Does the Branly effect occur in spark plasma sintering? Journal of Physics D: Applied Physics, 44(2).

[11] Olevsky E., Froyen L. (2006). Constitutive modeling of spark-plasma sintering of conductive materials. Scripta materialia, 55(12), 1175-1178.

[12] Zhang, Z., Liu, Z., Lu, J., Shen, X., Wang, F., Wang, Y. (2014). The sintering mechanism in spark plasma sintering - Proof of the occurance of spark discharge. Scripta materialia, 81, 56-59.

[13] Ge, Lihao. (2014). *Processing of uranium dioxide nuclear fuel pellets using spark plasma sintering.* (Doctoral dissertation, University of Florida).

[14] Myers, Rusty. (2006). The Basics of Physics. Westport, Connecticut: Greenwood Publishing Group.

[15] Egerton, R.F. (2005). Physical principles of electron microscopy: an introduction to TEM, SEM, and AEM. Springer.

[16] Maitland, T., Sitzman, S.. Electron backscatter diffraction (EBSD) technique and materials characterization examples. Springer.

[17] Paplewski, Peter. (2015). Fundamentals, overview, and applications of CS ONH analysis [powerpoint slides]. Bruker Elemental.

[18] Hafner, Bob. (2004). Energy Dispersive Spectroscopy on the SEM: A primer. University of Minnesota.

[19] Kaufmann, A., Cullity, B., Bitsianes, G. (1957). Uranium-Silicon Alloys. Journal of Metals, 27.

[20] Snelgrove, J.L., Domagala, R.F., Hofman, G.L., Wiencek, T.C. (1987). The Use of U3Si2 Dispersed in Aluminum in Plate-type Fuel Elements for Research and Test and Reactors. Argonne National Laboratory, Argonne, Illinois, USA.

[21] Harp, Jason M., Lessing, Paul A., Park, Blair H., Maupin, Jakeob. (2013). Preliminary Investigation of Candidate Materials for use in Accident Resistant Fuel. Idaho National Laboratory, Idaho Falls, Idaho, USA.

[22] Domagala, R.F. (1986). Phases in U-Si Alloys. Argonne National Laboratory, Argonne, Illinois, USA.

[23] Yemel'Yanov, V.S., Yevstyukhim, A.I. (1969). The Metallurgy of Nuclear Fuel: Properties and Principles of the Technology of Uranium, Thorium, and Plutonium. Pergamon Press.

[24] Oliver, Miquel. (2011). *Production of Mixed U-Zr Nitride Nuclear Fuel Powders from Metallic U-Zr Alloys.* (Master Thesis, KTH Royal Institute of Technology, Stockholm, Sweden).

[25] Yeon, Soo Kim. (2012). Uranium Intermediate Fuels (U-Al,U-Si,U-Mo). Argonne National Laboratory, Argonne, Illinois, USA.

[26] Hollmer, Tobias. (2011). *Manufacturing methods for (U-Zr)N-fuels* (Master thesis, KTH Royal Institute of Technology, Stockholm, Sweden).

[27] Hausner, H.H., Zambrow, J.L. (1956). The powder metallurgy of uranium. Sylvania Electric Products.

[28] Malkki, Peter., Jolkkonen, Mikael., Hollmer, Tobias., Wallenius, Janne. (2014). Manufacture of fully dense uranium nitride pellets using hydride derived powders with spark plasma sintering. Journal of Nuclear Materials, 452(1-3), 548-551.

[29] Guyadec, F.L., Genin, X., Bayle, J.P., Dugne, O., Duhart-Barone, A., Ablitzer, C. (2010). Pyrophoric behavior or uranium hydride and uranium powders. Journal of Nuclear Materials, 396(2-3), 294-302.

[30] Johnson, Kyle. (2012). *Formation of Solid Solution in Mixed Nitride Fuels.* (Master thesis, KTH Royal Institute of Technology, Stockholm, Sweden).

[31] Basu, Bikramjit. Some fundamentals on spark plasma sintering as a processing tool to fabricate biomaterials [Powerpoint slides]. Department of Materials Science and Engineering, Indian Institute of Technology Kanpur.